Check for updates

Crustal attenuation structure of the Tianshan tectonic belt and its spatiotemporal variations

Jin Li[1,2,3]*, Haikun Jiang[4] and Qiong Wang[2]

[1]Xinjiang Pamir Intracontinental Subduction National Field Observation and Research Station, Urumqi, China, [2]Earthquake Agency of Xinjiang Uygur Autonomous Region, Urumqi, China, [3]Urumqi Institute of Central Asia Earthquake, China Earthquake Administration, Urumqi, China, [4]China Earthquake Networks Center, Beijing, China

The quality factor value (Q) of the crustal medium, which can describe the anelasticity within the Earth's interior, is a sensitive indicator of changes in the crystalline structure induced by temperature and phase transformations. Although the velocity structure of the Tianshan region in Central Asia has been extensively studied, studies regarding its Q values are limited. These studies focus mainly on the crustal attenuation structure of the Tianshan region; however, their results are limited to the qualitative analyses of the local areas or averages over large areas. Therefore, in this study, we conducted seismic attenuation tomography to create a Q map of the crust underneath the Tianshan tectonic belt (TTB) at a resolution of 0.8° × 0.8° using data from 24,273 near-source waveforms recorded by 51 observation stations of the Xinjiang regional seismic network from 2009 to 2020. The regional distribution of the static and sliding-average values (Q_S) was calculated. The average value (Q_0) of TTB was approximately 523. Additionally, Q_s exhibited considerable lateral variations that strongly correlate with the surface tectonics of the TTB region. Furthermore, the velocity and attenuation structures of the TTB were positively correlated. The main part of the TTB exhibited high velocities and Q (indicating low attenuation), whereas the areas adjoining the Tarim and Junggar basins (at the South and North of the TBB, respectively) and their margins exhibited low velocities and Q (indicating high attenuation). This suggested that the attenuation structure of the TTB was highly consistent with its velocity and density structures. Since 1900, most earthquakes in the TTB having magnitudes ≥6.0 earthquakes have occurred at the junctions of high- and low-Q-value areas, or in areas with low Q values. According to the Q_s values in different periods, the average Q_s of the entire TTB only varied between 500 and 540. However, the average Q_s in the middle TTB region portrays an upward trended over time (from 494 in 2010 to 554 in 2020). The average Q_s of the southwestern TTB region has been relatively stable, varying between 490 and 530. The Q_0 of the southwestern TTB region was lower than that observed in the middle TTB region in most of the time. This observation is more consistent with the tectonic activity recorded in the southwestern TTB region (with greater intensity) than that observed in the middle Tianshan. In addition, the number of earthquakes with magnitudes ≥4.0 correlated positively with the regional average Q_s in the middle and southwestern Tianshan. Notably, the higher the regional average Q value, the larger the number of moderate earthquakes. This correlation suggests that in

Abbreviations: Quality factor value (Q), Three-dimensional (3D), Two-dimensional (2D), Tianshan tectonic belt (TTB), Arrival time difference (ATD), Attenuation operator ($t*$), Sliding-average value (Q_s), Average value (Q_0).

earthquake-prone regions, the accumulation and release of stress influence the opening or closure of crustal fractures, resulting in noticeable changes in the Q values. The findings of our study provide novel insights into the mechanisms of earthquakes and their correlation with the structure of the Earth's crust.

1 Introduction

The attenuation of seismic waves in the Earth's crust is caused by geometric diffusion and crustal anelasticity (Liu et al., 2004a), which, in the lithosphere, is generally expressed by the rock quality factor value (Q) (Liu et al., 2004b; Wang et al., 2007; Hao et al., 2009). The characteristics of the crustal attenuation structure are closely related to the structural characteristics of the crust, e.g., the intensity of tectonic movements, distribution of active structures, velocity structure of the crust, thickness of the sedimentary layer, and properties of the crustal medium (Pei et al., 2006; Pei et al., 2008; Wang et al., 2007; Ma et al., 2007; Sun et al., 2012). For example, regions with intense tectonic activity are associated with a low Q value since seismic waves are considerably attenuated by fluids that fill fractured rocks and voids. Meanwhile, regions with stable crustal medium are generally associated with high Q values, as the seismic waves only lose a small amount of energy when propagating through these rocks (Walsh, 1966; Tapponnier and Molnar, 1979; Mitchell, 1995; Mitchell et al., 1997; Hu et al., 2003; Pei et al., 2010). Compared with the velocities of seismic waves, the Q value is more sensitive to changes in the structure of the lithosphere and its properties (Wang et al., 2007). For instance, the lateral variations in Q within the crust and upper mantle may exceed 100%, whereas those in velocity typically do not exceed 10% (Romanowicz, 1990; Romanowicz, 1994). Therefore, studies on the variations in the Q values within regional crustal media can provide insights into its structural characteristics and properties. Theoretically, Q can be expressed as a function of three-dimensional (3D) spatial coordinates. However, as Q is affected by the 3D velocity structure, errors in the velocity structure can be transferred to Q, resulting in inaccurate 3D Q-tomography (Su, 2009; Ye et al., 2018; Hu, 2020). In general, two-dimensional (2D) Q-tomography is performed by calculating the weighted average of the Q values in various depths; therefore, the results of this method can accurately reflect the lateral variations in Q. Indeed, recent studies that use 2D Q-tomography to investigate the lateral variations in crustal attenuation structure have provided several novel insights (Pei et al., 2006; Pei et al., 2008; Pei et al., 2010; Wang et al., 2007; Sun et al., 2012).

Studies on the crustal attenuation structure underneath the Tianshan tectonic belt (TTB) region in Central Asia have been hampered by the relatively slow development of a seismic network in Xinjiang Province, China. Our limited understanding of the crustal attenuation structure underneath the TTB is predominantly derived from the qualitative analyses of local areas, or the results averaged over large areas. Non-etheless, the western section of Tianshan is associated with a low Q value (high attenuation), whereas the eastern section is associated with a high Q value (low attenuation). The western and eastern sections of the Tarim Basin exhibit low and high

seismic attenuations, respectively (Wang et al., 2008). Previous studies have calculated the average Q values of the local areas within the Tianshan region. For example, Jiang et al. (2007) obtained a Q_0 value of 344 for the northern Tianshan region, whereas Liu and Li. (2014) reported 465 for the same region. Zhao et al. (2011) calculated a Q_0 value of 460 for the middle Tianshan region, while Li et al. (2010) reported 213 for the southwestern Tianshan region, using Atkinson's method (Atkinson and Mereu, 1992). The development of the Xinjiang regional seismic network has increased the number of digital seismic stations in the Tianshan region. Owing to the frequent seismic activity in Xinjiang (approximately 40% of the earthquakes in China occur in this province), these stations provide sufficient data for studying the crustal attenuation structure of the Tianshan region. In this study, we performed Q tomography for the Tianshan region, through the tomographic inversion of the high-frequency attenuation operator, t^* (Zhou et al., 2009). By analyzing the spatiotemporal variation in the Q values in the TTB, we could elucidate the correlation between the structural characteristics and deep dynamics of the TTB and those of its adjacent blocks.

2 Geological setting of the Tianshan tectonic belt (TTB)

The TTB is 2,500 km in length, approximately two-thirds of which is located in the Chinese province of Xinjiang (Figure 1). The TTB also borders the Tarim and Junggar basins, at the south and north, respectively. During the Paleozoic era, the TTB experienced supercontinental rifting, the breakup of the North and South Tianshan oceans, continuous expansion of the ocean basin and continental block, subduction and subsidence of the oceanic crust, and plate collision-suture (Liu et al., 2011). During the early Cenozoic period, the convergence between the Indian and Eurasian plates was accommodated by crustal shortening at the Tibetan Plateau and Tianshan region and the eastward extrusion of the eastern Tibetan Plateau (Molnar and Tapponnier, 1975; Molnar and Tapponnier, 1978; Tapponnier and Molnar, 1977; Tapponnier and Molnar, 1979; Molnar and Lyon-Caen, 1989; Zhang et al., 1996; Shu et al., 2004; Zhao et al., 2021). Owing to intense crustal shortening, extrusion deformation, and tectonic upliftment, the TTB is the most active intracontinental orogenic belt in mainland China (Feng, 1985; Deng et al., 1991). These tectonic movements cause frequent earthquakes of high magnitude in the TTB region. Indeed, since the beginning of the 20th century, 11 earthquakes of magnitudes ≥7 have occurred in the TTB, the strongest of which was the Artux earthquake in 1902 (magnitude of 8¼). Since the turn of the century, 15 earthquakes of magnitudes ≥6 have occurred in the TTB. Based on global

FIGURE 1
Map illustrating the Tianshan tectonic belt (TTB) and its adjacent tectonic units, along with the geographical distributions of the historical earthquakes and seismic observation stations in the region. The earthquakes having Ms ≥ 6.5 that occurred between 1900 and 2000 are indicated by gray circles, while the earthquakes of Ms ≥ 6.0 that occurred after 2000 are indicated by blue circles. The dotted line represents the border between the middle and southwestern TTB. F1: Borohoro–Aqikekuduke fault; F2: Beiluntai fault; F3: Northern Ili Basin margin (Kashi River) fault; F4: Nalati fault; F5: Yilianhabierga fault; F6: Kumugeremu fault; F7: Maidan–Shayilamu fault; F8: Kalpintag fault; F9: Piqiang fault; F10: Kangxiwa fault; F11: Kongur fault; F12: Oytak fault; F13: Karakoram fault; F14: Talas–Fergana fault; F15: Kazkeaerte fault; F16: Tiklik fault.

navigation satellite system data, rapid crustal shortening in the S–N direction is the defining characteristic of present-day tectonic activity in the TTB (Abdrakhmatov et al., 1996; Larson et al., 1999; Wang et al., 2000; Larson et al., 2003; Zhang et al., 2003). The rate of this S-N trending convergence gradually increases from East to West, along the TTB, with extrusion and shortening deformations primarily occurring in the areas adjoining the basins to the South and North. Therefore, the TTB has an uneven distribution of surface deformation (Wang et al., 2000; Reigber et al., 2001).

Unique tectonic movements and frequent strong earthquakes have highlighted the importance of the TTB as an ideal location for promoting global studies on continental dynamics (Tapponnier and Molnar, 1977; Avouac et al., 1993; Roecker et al., 1993; Shu et al., 2004; Jolivet et al., 2010; Johnston et al., 2012; Liu et al., 2012; Deev and Korzhenkov, 2016; Cai et al., 2019). In recent years, several studies have been conducted on the TTB, which created a basic sketch of the TTB's general tectonic framework. The crustal structure of the TTB, obtained by inverting artificial seismic reflection profiles, demonstrates that the Tarim Basin subducts northward under the TTB and that the Junggar Basin in the north experiences a strike-slip contact with the TTB (Lu et al., 2000; Gao et al., 2002; Xiao et al., 2004; Guo et al., 2006). As the basins to the South and North of TTB consist of rigid blocks, with an intact lithospheric structure, they exhibit high seismic wave velocities. In contrast, the TTB is a fragmented block that portrays low velocities (Zhao et al., 2021), while the crust-mantle structure in the TTB is complex and its unique tectonic movements have resulted in lateral non-uniformities in its medium properties and structural tectonics (Liu et al., 2011). Using dense array data,

several studies have inverted the fine S- and P-wave velocity structures in the crust and upper mantle across the TTB and revealed significant deformation in the S–N direction, rock bodies with marked low S-wave velocity, and an arrangement of bodies with alternating high and low velocities in the crust beneath the TTB (Shao et al., 1996; Guo et al., 2006; Li et al., 2007; Xiong et al., 2011). Furthermore, the lithosphere under the TTB is relatively thin, which may be related to processes, such as continental collision-suture and delamination, along with the upliftment of the orogenic belt and subsidence of Moho (Schubert et al., 2001; Kumar et al., 2005; Liu, and Guo et al., 2007).

However, several of the abovementioned studies present inconclusive, or even contradictory, findings. The Q value is closely related to the structural characteristics of the crust, such as the distribution of faults in tectonically active regions, intensity of tectonic movement, distribution of magma in volcanic regions, and intracrustal low-velocity layers (Ma et al., 2007). Q-tomography can provide novel insights into the crustal structure of the TTB and help resolve the ambiguities in the current literature.

3 Methodology

Digital seismic waveforms contain information about seismic hypocenters, seismic-wave propagation paths, and the site response of seismic stations. The factors responsible for the attenuation of seismic energy along its path of propagation include geometric attenuation and medium anelasticity (Liu et al., 2003; Zhou et al., 2009; Wang et al., 2012a; Wang et al., 2012b; Wang et al., 2016; Li et al., 2017).

In the frequency domain, the amplitude spectrum of the ith seismic event observed at the jth station, $A_{ij}(f)$, can be expressed as follows (Sherbaum, 1990):

$$A_{ij}(f) = S_i(f)I_j(f)R_j(f)G_{ij}(f)B_{ij}(f) \qquad (1)$$

where f is the frequency, $S_i(f)$ is the seismic source spectrum, $I_j(f)$ is the instrument response function, $R_j(f)$ is the site response, used to characterize the amplification of seismic waves by the surface stratum near the station, $G_{ij}(r)$ is the geometric diffusion term, and $B_{ij}(f)$ is the attenuation spectrum.

The source spectra were analyzed using the ω^2 source model (Brune, 1970), in which the source spectra were described using the low-frequency asymptote (Ω_0) and corner frequency (f_c), such that $S_i(f) = \Omega_0/[1 + (\frac{f^2}{f_c^2})]$. The geometric diffusion factor can be expressed by the trilinear attenuation function proposed by Atkinson and Mereu. (1992):

$$G_{ij}(r) = \begin{cases} r^{-b_1}, & r \le R_{01} \\ R_{01}^{-b_1}R_{01}^{b_2}r^{-b_2}, & R_{01} < r \le R_{02} \\ R_{01}^{-b_1}R_{01}^{b_2}R_{02}^{-b_2}R_{02}^{b_3}r^{-b_3}, & r > R_{02} \end{cases} \qquad (2)$$

In the geometric attenuation model, the coefficients b_1, b_2, and b_3 are frequency independent. When $r \le R_{01}$, the corresponding direct wave geometric attenuation. When $R_{01} < r \le R_{02}$, it corresponds to the transition zone. Within the range of this source distance, the reflection wave on the discontinuity and Moho in the crust is added to the direct wave. When $r > R_{02}$, it corresponds to the attenuation of the S wave reflected by multiple refractions.

The attenuation spectrum along the entire ray path, $B_{ij}(f)$, may be expressed as follows (Sherbaum, 1990; Sanders et al., 1993):

$$B_{ij}(f) = \exp\left(-\pi f t_{ij}Q_{ij}^{-1}\right) = \exp\left(-\pi f t_{ij}^*\right) \qquad (3)$$

where t_{ij} is the travel time along the ray path, Q_{ij} is the dimensionless quality factor, and t_{ij}^* is the operator along the entire ray path (i.e., the attenuation operator t^*).

As the seismic stations selected for this study were from Xinjiang regional seismological network, all set up on bedrock, their site responses were assumed to be 1 (Zhou et al., 2009); the instrument response was removed directly, using the stations' parameters. Under this condition, the amplitude spectrum can be expressed as $A_{ij}'(f) = A_{ij}(f)/I_j(f)$, and Eq. 1 can be rewritten, as follows:

$$A_{ij}'(f) = \Omega_0 \frac{f_c^0}{f_c^0 + f^2} G(r) \exp\left(-\pi f t_{ij}^*\right) \qquad (4)$$

The t_{ij}^* operator can also be expressed as the projection of $1/[Q(s)v(s)]$ along the ray path from the seismic source i to the station j (Cormier, 1982; Wittlinger et al., 1983), as shown below:

$$t_{ij}^* = \int_{path} \frac{1}{Q(s)v(s)} ds \qquad (5)$$

where v is the S-wave velocity and ds is the unit ray path.

Equation 4 contains three unknown variables, namely, Ω_0, f_c, and t_{ij}^*. The attenuation along the path from the seismic source to each station, t_{ij}^*, can be calculated via inverting the seismic displacement spectrum, based on Eq. 4, whereas Ω_0 and f_c depend solely on the seismic source. In this study, the Levenberg–Marquardt method was used for spectral inversion (Hansen et al., 2004). Q-tomography was

performed based on Eq. 5, using the same method as travel time tomography (Sherbaum, 1990; Haberland and Rietbrock, 2001; Wang et al., 2012a; Wang et al., 2016; Li et al., 2017).

The waveform data used in this study were obtained from 51 digital seismic stations in the TTB (Figure 2). First, we applied bandpass filtering and mean removing to the two horizontal components of the seismic waveforms and selected the S-wave and noise windows; the period containing 90% of the S-wave energy was selected as the S-wave window (Su, 2009). At near-source distances, the S-wave window only contains the direct S-wave. At longer epicentral distances, the S-wave window contains the waves reflecting off the intracrustal and Moho discontinuities. At very long distances, the S-wave window contains the Sn and Lg phases. The length of the S-wave window is directly proportional to the epicentral distance [or the arrival time difference (ATD)]. In other words, the length of the S-wave window increases with the epicentral distance (or ATD) (Li et al., 2010; Zhao et al., 2011; Liu, and Li, 2014). We manually recorded the "S wave window" of 721 original waveforms (Figure 3), and then fitted the "S-wave window" to epicentral distance relationship with a linear fit of the form $y = 1.06x + 22.6$, where y is the S-wave window and x is the epicentral distance (Sg-Pg). The selection of the noise window was performed by considering the waveform records prior to the arrival of the P-wave. The time-domain waveform data were converted into frequency-domain amplitude spectra, using the fast Fourier transform. Since all the seismometers at the stations selected in this study were velocity meters, the velocity-amplitude spectra were also converted to displacement spectra. To eliminate the seismic data having low signal-to-noise ratios (SNR), we used only the seismic data having an SNR of >2 (i.e., with an amplitude at least twice that of the noise) observed by a minimum of four stations in our subsequent calculations.

Suppose that an earthquake was recorded by n stations. As Ω_0 and f_c depend solely on the seismic source, a total of $(n + 2)$ unknowns (i.e., Ω_0, f_c, $t_1^*, \ldots, t_n^*$) were inverted, using Eq. 4. We assumed that there are m frequency points and used $A_i^{obs}(f_j)$ and $A_i^{cal}(f_j)$ to denote the observed and theoretical amplitude spectra, respectively, at the ith station and jth frequency points. The inversion of the observed spectra at multiple stations were used to determine the values of the unknown variables that minimize the residual $\sum_{i=1}^{n}\sum_{j=1}^{m} \lg |A_i^{obs}(f_j) - A_i^{cal}(f_j)|$.

In this study, we employed a genetic algorithm to invert the $(n + 2)$ unknowns, to minimize the sum of the residuals between the observed and theoretical spectra at all the stations and frequency points (Liu et al., 2003). Based on the spectral inversion of noise- and geometry-corrected waveforms collected by multiple stations for the same seismic event, we could infer that the high-frequency attenuation of the displacement spectra was predominantly determined by the Q value of each path. Previous studies demonstrate that the high-frequency part of the noise spectrum has a high amplitude at frequencies above 15 Hz, which often decreases the SNR of displacement spectra to levels below the predetermined SNR criterion (Su et al., 2006). Therefore, the spectral inversions were constrained to 1–15 Hz (Zhou et al., 2009).

Notably, 2D Q-tomography may be viewed as the projection of a weighted average of Q values at different depths onto a plane. As a dominant focal depth will be present in any distribution of seismic events, the results of 2D Q-tomography correspond to the lateral
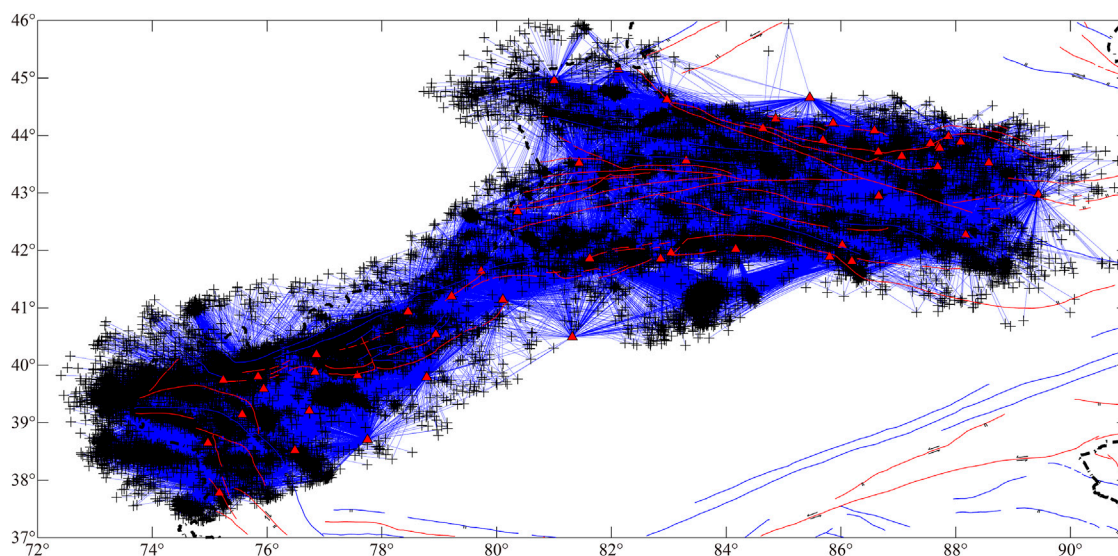
FIGURE 2
Distribution of seismic observation stations (red triangles), events (+), and rays in the Tianshan tectonic belt (TTB).
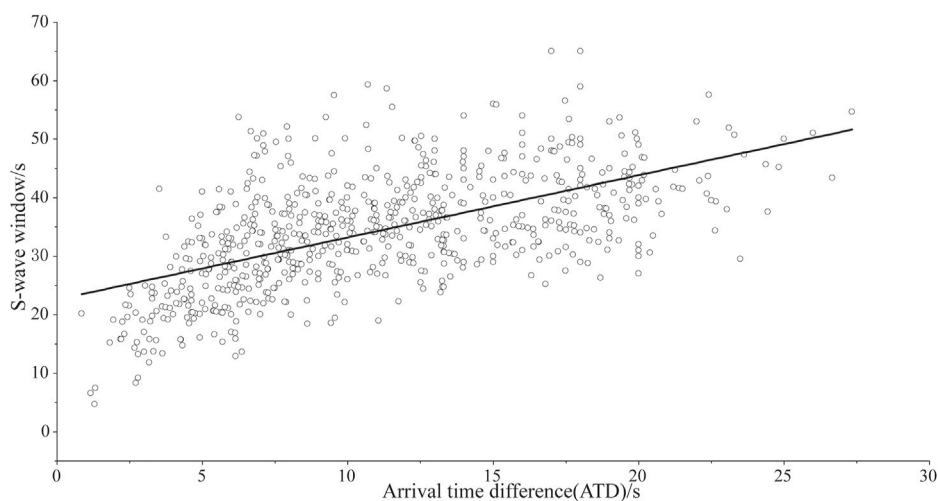
FIGURE 3
Graph showing the fitted relationship between the S-wave window and epicentral distance.

distribution of the average crustal Q values above the dominant focal depth (Su, 2009; Ye et al., 2018).

4 Conducting Q-tomography based on S-wave attenuation in the Tianshan tectonic belt (TTB)

4.1 Data and solution stability analysis

In this study, for the static Q-tomography of the TTB, we used the observational data recorded by the Xinjiang regional seismic network from 2009 to 2020. During this period, a total of 24,273 locatable seismic events having magnitudes of 2.0–5.4 (M_L 2.0–5.4) were recorded by 51 digital seismic stations in the Tianshan seismic zone (Figure 2). A total of 145,368 t^* data records with high SNR were acquired through inversion, using the method described in the previous section. Previous studies have shown that the Q_0 value of a region generally ranges from several tens to hundreds (Wang et al., 2012a), but may exceed 1,000 in rare cases (Mitchell et al., 1997; Baqer and Mitchell, 1998). Therefore, the data were first filtered by removing the t^* data records having overly low values (specifically, a t^* data record was removed when the epicentral distance/t^* was greater than 4,000). If the intracrustal velocities
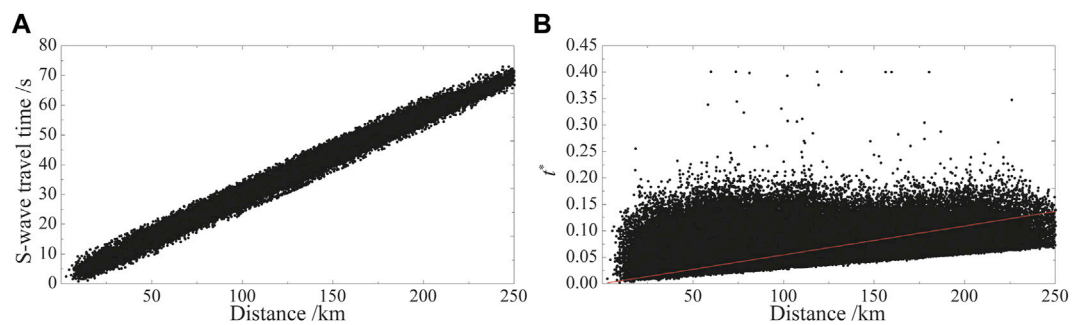
FIGURE 4
Linear fit of **(A)** arrival time difference (ATD) and **(B)** attenuation operator (t^*) data to the epicentral distance.
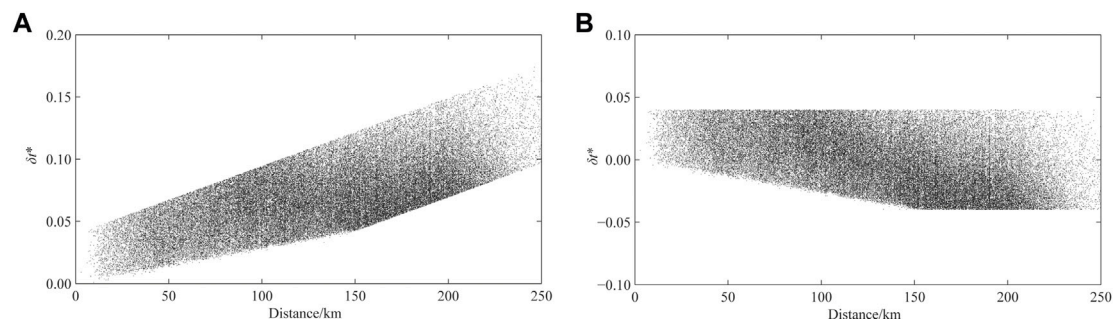
FIGURE 5
Variation in the residual with epicentral distance, **(A)** before and **(B)** after inversion.

within the TTB are uniform, the linear fitting of the travel time-epicentral distance graph (Figure 4A) will yield an average crustal S-wave velocity ($\bar{v}_s$) of 3.49 km/s. Then, t^* is linearly fitted to the epicentral distance (Figure 4B), which yielded an average crustal Q_0 value of 523 for the TTB. As Q_S measurements inherently contain large errors, we considered only the data points whose observed values differed from the corresponding fitted values by ≥ 1 standard deviation (0.0403). Notably, 77,852 t^* data records met this requirement. Figure 2 portrays the distribution of the corresponding rays. Based on the t^* data, the crust beneath the TTB (37°–45.5° N, 72°–90.5° E) was divided into uniform cells. Q_S inversion was performed, at the resolution of $0.8° × 0.8°$, with each cell having an average of 1,252 rays. Q_0 and $\bar{v}_s$ were used as initial values for tomographic inversion. Furthermore, we performed 10 iterations of the ray-tracing pseudo-bending method, to obtain the Q value of the region. The root-mean-square residual of t^* decreased from 0.0216, before inversion, to 0.0198, after inversion. Figure 5 illustrates how the residual varied with the epicentral distance, before and after the inversion.

To test the stability of the inversion results of Q_0 value, 20% Gaussian noise, with a mean of 0 and variance of 1, was added to the original t^* data (Pei et al., 2010), i.e., $T^* = t^* × (1+20\%gasdev)$ where t^* is the original data, T^* is the data after noise is added, and gasdev is a function with a mean value of 0 and a variance of one Gaussian distribution. The data with added noise were inverted using the same

parameters as the actual inversion, and the error of Q_0 value was obtained. For 50 times of noise synthesis data—inversion operation, the error result of Q_0 value is not more than 14 (2.67% of the average Q_0).

4.2 Checkerboard resolution test

A checkerboard resolution test was performed, to determine whether the tomographic inversion for the $0.8° × 0.8°$ grids was reliable (Figure 6). As shown in Figures 2, 6, the TTB is densely covered with rays, and the resolution is high. False resolution only occurred in a few areas at the edges of the rays.

4.3 Static Q-tomography based on S-wave attenuation

Lateral variations in Q are associated with the thickness of the sedimentary layer, intensity of crustal movements, and nature of the medium (Sun et al., 2012). In this study, we performed Q-imaging of the Tianshan crust through attenuation tomography, at a resolution of $0.8° × 0.8°$, using seismic data from January 2009 to December 2020 (Figure 7). The value of Q_S ranged from 300 to 800, with an average Q_0 value for the entire TTB of 523. This result is consistent
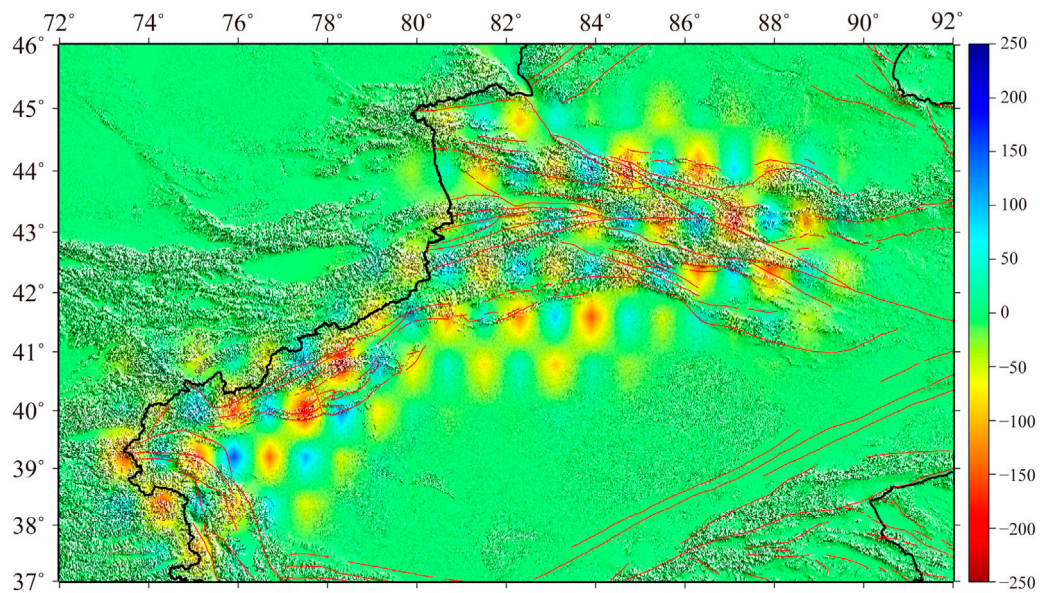
FIGURE 6
Results of the checkerboard resolution test.
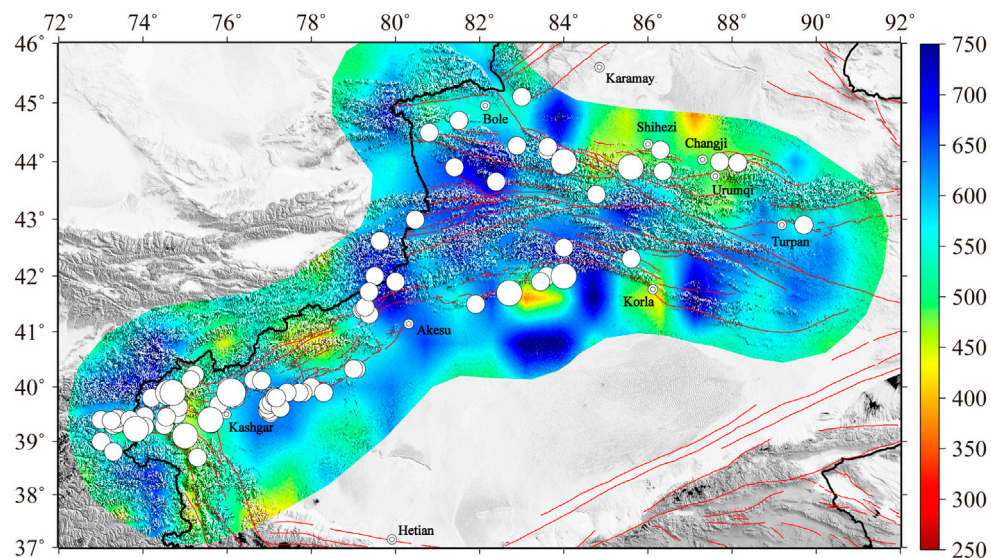
FIGURE 7
Distribution of S-wave-derived Q values for the Tianshan tectonic belt (TTB) in 2009–2020. White circles indicate the epicenters of earthquakes of magnitudes ≥6.0 that occurred after 1900.

with the average Q_0 value (520) reported by Li et al. (2017) for the middle Tianshan region using the same method, but higher than the average Q_0 value (460) for the middle Tianshan region reported by Zhao et al. (2011).

The crustal Q values of the TTB region exhibited significant lateral variations (Figure 7). The distribution of these Q values and the corresponding variations in crustal attenuation were strongly associated with surface tectonics in this region. The main area of the TTB exhibited high Q values, whereas the parts adjacent to the basins in the south and north and the basin margins were characterized by low Q values, which was in line with the results obtained for other regions of China (Wang et al., 2008; Sun et al., 2012). For example, the regions having thick sedimentary layers, such as the North China Plain, Songliao Basin, and Hailar Plain, are

associated with low Q_0 values (high attenuation), whereas regions, such as the Yanshan, Taihang, and Xingmeng fold belts, exhibited high Q_0 values (low attenuation), due to the presence of thin sedimentary layers or bedrock outcrops (Sun et al., 2012).

The area in the middle Tianshan region, between the Borohoro (F1) and the Beiluntai (F2) faults (termed zone V_1 in this study) (Figure 1), constituted the main area of the TTB and had high Q values (650–750). The areas having low Q values (generally below 550) were primarily located adjacent to basins on the southern and northern sides of the TTB. In these areas, the medium gradually transitions from hard mountainous rock to soft sedimentary layers. Interestingly, a unique distribution of Q values was observed (Figure 7) in southwestern TTB (termed zone V_2 in this study) (Figure 1). Specifically, there was a considerable difference in the Q values of the eastern and western sides of the Piqiang fault (F9), wherein the stations recorded low and high Q values in the eastern and western sides of the fault, respectively. The F9 fault portrayed a near S–N strike and was approximately perpendicular to the thrust nappe tectonic system of Kalpin, which separated it into eastern and western sections. Studies have shown that the eastern and western sides of the Kalpin thrust nappe tectonic system have tremendously different deformation rates; as the nappes in the western section generally exhibit higher slip rates than those in the eastern section. Furthermore, the difference in the slip rates increases with the proximity to the front (Ran et al., 2006; Yang et al., 2006; Li et al., 2016). Yang et al. (2008) have proposed that the F9 fault is a deep and large fault running through the base of the Tarim Basin, and that the Tarim Basin separates into two rock sheets in front of the southwestern TTB, subducting below the Tianshan Mountains. These factors lead to significantly more frequent and stronger earthquakes on the west side of the F9 fault, compared with its east side (Tang et al., 2013), resulting in a disparity in the Q values between its eastern and western sides. In addition, markedly low Q values were observed near the Pamir knot, which is known for extremely strong tectonic movements.

The low Q values partly reflect the intensity of tectonic activity in these areas. These low-Q areas of the TTB resemble the Himalayan fold belt on the southern margin of the Tibetan Plateau and the Yunnan–Tibet fold zone, in terms of their tectonic characteristics. Due to the collision and extrusion between the Indian and Eurasian plates, these areas experience intense tectonic activity, as well as continuous crustal thickening and plateau uplifting, which makes them susceptible to strong earthquakes (Cong et al., 2002). Conversely, tectonically stable regions are often associated with high Q values. For example, the Q values of the Siberian Platform (Mitchell et al., 1997) and the eastern United States of America (Baqer and Mitchell, 1998) can be >1,000.

Although the drivers of the lateral Q variations in the TTB require further investigation, it is generally believed that Q is closely related to the fractures in the medium and their degree of fluid filling. Tectonically active regions are associated with very low Q values because the medium is fragmented and contains a large number of fractures (Hu et al., 2003; Ma et al., 2007; Qiu et al., 2021). At high crustal fracture densities, fluids can flow freely into and

through the fractures, thereby attenuating seismic waves (Mitchell, 1995).

Most of earthquakes with magnitudes ≥6.0 that have occurred in the TTB since 1900 are located in the transition zones between the high- and low-Q areas, or in the low-Q areas (Figure 7), e.g., the Pamir syntaxis that has a high density of earthquakes having magnitudes ≥6.0. Generally, it is believed that energy does not easily accumulate within a homogeneous crustal medium. As transition zones between high- and low-Q areas are areas of convergence between "soft" and "hard" materials, they can facilitate the accumulation of strain energy, resulting in earthquakes (Wang et al., 2012a; Ye et al., 2018). In addition, the area west of the F9 fault consisted of a junction between three tectonic systems, namely, the Tarim Basin and the Tianshan and West Kunlun Mountains; this area had a substantially higher Q value than that of the areas to its east and west. Notably, more than 10 strong earthquakes (magnitude ≥6) had occurred in this area during 1997–2003, collectively known as the Jiashi strong earthquake swarm (Zhao et al., 2008). Such earthquake swarms are rare in mainland China and the rest of the world V_2. Most low-Q areas in the TTB are tectonically active.

4.4 Dynamic Q-tomography based on S-wave attenuation

To analyze the spatiotemporal variations in the Q values in the TTB in greater detail, the seismic data for the study area were divided into six 2-year periods (2009-2010, 2011-2012, 2013-2014, 2015-2016, 2017-2018, and 2019-2020). The calculation for each period involved 10,500–16,000 t^* records, and there were 160–260 rays in each cell (Table 1). The average Q_0 value of the TTB in each period ranged from 500 to 540, which was comparable to the average Q_0 value (523) for the entire study period (2009–2020). In addition, the method of adding Gaussian noise to t^* data was used to obtain the errors of Q_0 values at different time periods (Table 1).

Figures 8A–F illustrate the lateral Qs variations in the TTB for each time period, indicated by a red–blue gradient; red indicates the areas having Qs values below the mean Q_0 value (high attenuation), whereas blue indicates the areas having Qs values above the mean Q_0 value. For comparison, the Q_0 values for the abovementioned periods were used to calculate the lateral variation based on an average value of 523. The overall distribution of Q in the TTB did not significantly vary from one period to another. The high-Q-value areas were located primarily in the main TTB area, whereas the low-Q-value areas were predominantly located in the areas adjacent to the basins located to the South and North of the TTB, as well as those near the Pamir syntaxis in Zone V_2 and the area east of the F9 fault. These results also proved the stability of the tomography results, as the period-wise tomographic inversions were generally consistent with the tomographic inversion for the entire study period. Notably, on the outer edges of the rays, the smearing effect resulted in a false resolution and potentially inaccurate Q values at the margins of the study area (He et al., 2017). Therefore, the Q values in these margins are not discussed further.

TABLE 1 Data statistics for the six two-year periods (between 2009 and 2020) considered in this study.

Time period	Start and end time	Number of earthquakes	Total number of t* data points	Number of t* data points actually used	Average number of rays in grid cells	Residual of t* before inversion	Residual of t* after inversion	Q_0 values
I	2009.01~2010.12	3588	22863	12968	228	0.0234	0.0213	510
II	2011.01~2012.12	4267	24584	12881	222	0.0205	0.0187	530
III	2013.01~2014.12	4085	23103	12147	186	0.0295	0.0203	510
IV	2015.01~2016.12	3364	19217	10509	168	0.0229	0.0211	500
V	2017.01~2018.12	4142	25646	13350	188	0.0200	0.0184	530
VI	2019.01~2020.12	4826	29955	15886	255	0.0206	0.0185	530
Entire study period	2009.01~2020.12	24273	145368	77852	1252	0.0216	0.0198	520
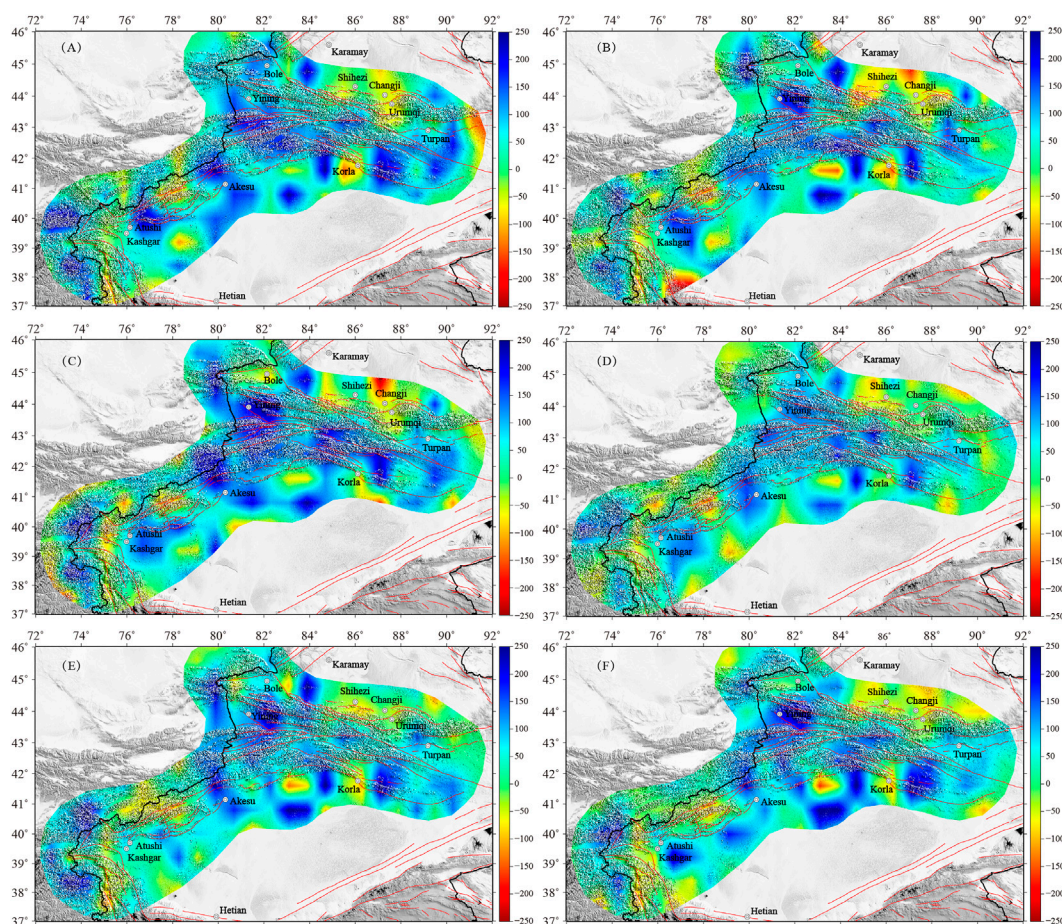
FIGURE 8
Temporal variations in the S-wave-derived Q values of the Tianshan tectonic belt (TTB) for the six 2-year periods considered in this study. **(A)** 2009-2010, **(B)** 2011–2012, **(C)** 2013–2014, **(D)** 2015–2016, **(E)** 2017–2018, and **(F)** 2019–2020.
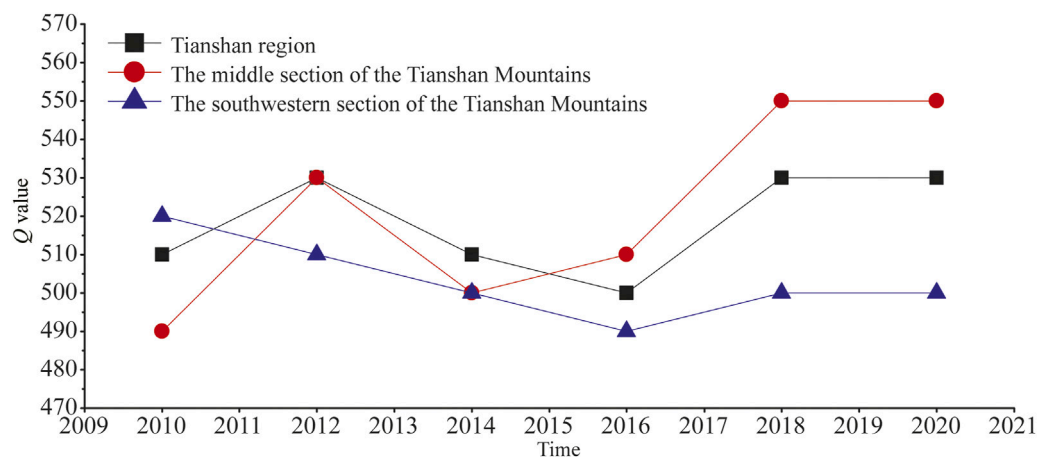
FIGURE 9
Temporal variations in the regional average Q values in the Tianshan tectonic belt (TTB), middle Tianshan (zone V_1), and southwestern Tianshan (zone V_2) regions.

4.5 Relationship between regional average Q and seismicity

Previous studies reported a positive correlation between seismicity and the regional average Q value (Pei et al., 2010; Wang et al., 2016). As the TTB exhibits significant lateral variations in Q, during the analysis it is often divided along the Kashgar–Aksu and Baicheng–Kuqa thrust systems to form two zones, namely, V_1 (middle Tianshan) and V_2 (southwestern Tianshan), which have distinct tectonic and seismic characteristics (Figure 1) (Yin et al., 1998; Chen et al., 2001). This zonation has been used in many previous studies (Yang et al., 2008; Gao et al., 2010; Qu et al., 2010; Wang et al., 2011). The temporal variation in the regional average Q of these zones is shown in Figure 9. The average Q value in zone V_1 (red curve) ranged from 490 to 560, showing an upward trend since 2009 (except for the 2011-2012 period). Conversely, the average Q value (blue curve) in zone V_2 was relatively stable, in the range of 490–530 for most of the study period. In addition, the average Q value in zone V_1 was higher than that of zone V_2 during most time periods (except for 2009-2010). The regions with intense tectonic activity and frequent strong earthquakes were characterized by low Q values (Hearn et al., 1991; Wang et al., 2007; Hearn et al., 2008; Wang et al., 2008; Wang et al., 2016; Ma et al., 2007; Pei et al., 2010). Haydar et al. (1990) have indicated that the active fault areas in the New Madrid seismic zone and its surrounding areas exhibited low Q values and strong seismic-wave attenuation, whereas the tectonically stable areas were associated with high Q values and weak attenuation. Our findings are in agreement with the results of Haydar et al. (1990); zone V_2 portrayed lower Q values than zone V_1, and the tectonic activity in zone V_2 was also more intense than that in zone V_1.

Regions with high stress accumulation are typically associated with frequent and intense seismic activities (Wan et al., 2009; Yi et al., 2013). Destabilization in a rock body occurs when the differential stress on a fault exceeds the rock fracture strength, resulting in an earthquake. Therefore, an increase in stress release often manifests as an increase in the seismic activity and earthquake frequency (Pei et al., 2010). Several studies have shown that the variations in the regional Q value tend to be strongly correlated with the local seismicity. In the Sichuan-Yunnan region, temporal variations in the regional average Q correlate significantly and positively with the number of earthquakes with magnitudes ≥4.5 that occurred during the corresponding period (Pei et al., 2010). In Hainan Island and its adjacent areas, the increase and decrease in the moving average Qs values generally coincide with the increase and decrease in the local earthquake frequency (Wang et al., 2016). Laboratory studies (Toksoz et al., 1979; Winkler and Nur, 1979) have shown that the Q value of a rock increases with its stress level, regardless of whether the rock is dry, or completely or partially saturated with water. Furthermore, Pei et al. (2010) noted that an increase in rock stress decreased the number of fractures, which in turn decreased the attenuation of seismic waves. In other words, the increase in seismic activity, accompanied by an increase in Q values, are external manifestations of stress accumulation.

Based on the abovementioned results, we tallied the numbers of moderate and strong earthquakes in zones V_1 and V_2 over the six 2-year time periods (Table 2). There was a strong positive correlation between the regional average Q and the number of earthquakes having magnitudes ≥4.0, in each zone and period (Figure 10). This result was consistent with the findings for the Sichuan–Yunnan region (Pei et al., 2010) and Hainan Island (Wang et al., 2016), where an increase in the Q value was generally accompanied by an increase in the number of earthquakes. However, the causal relationship between the Q value and the number of earthquakes remains ambiguous, because no existing studies could determine whether the increase in the earthquake frequency was caused by an increases in the Q value, or vice versa. In regions where moderate–strong earthquakes are frequent (e.g., the Sichuan–Yunnan region), some scholars are of the opinion that the former (increases in the Q value increase the earthquake frequency) is a better fit for their observations (Pei et al., 2010). That is, the pre-earthquake increase in stress can induce expansions in the rock volume (Scholz, 2002), resulting in the initiation, growth, and

TABLE 2 Earthquake numbers and Q_0 values observed in the middle and southwestern regions of the Tianshan Mountains.

Time period	$M_S \geq 3.0$		$M_S \geq 3.5$		$M_S \geq 4.0$		$M_S \geq 4.5$		Average Q_0 value/errors			
	Zone V_1	Zone V_2	Zone V_1	Zone V_2	Zone V_1	Zone V_2	Zone V_1	Zone V_2	Q_0 of Zone V_1	errors	Q_0 of Zone V_2	errors
2009–2010	80	114	27	44	12	22	3	6	490	13	520	13
2011–2012	119	98	52	33	24	17	10	8	530	16	510	14
2013–2014	102	118	30	33	12	12	3	6	500	12	500	14
2015–2016	118	173	43	45	24	18	9	7	510	15	490	11
2017–2018	174	122	53	39	30	18	14	9	550	18	500	13
2019–2020	156	137	50	51	25	25	13	13	550	17	500	13

*Notes: Zones V_1 and V_2 refer to the middle and southwestern sections of the Tianshan Mountains, respectively.
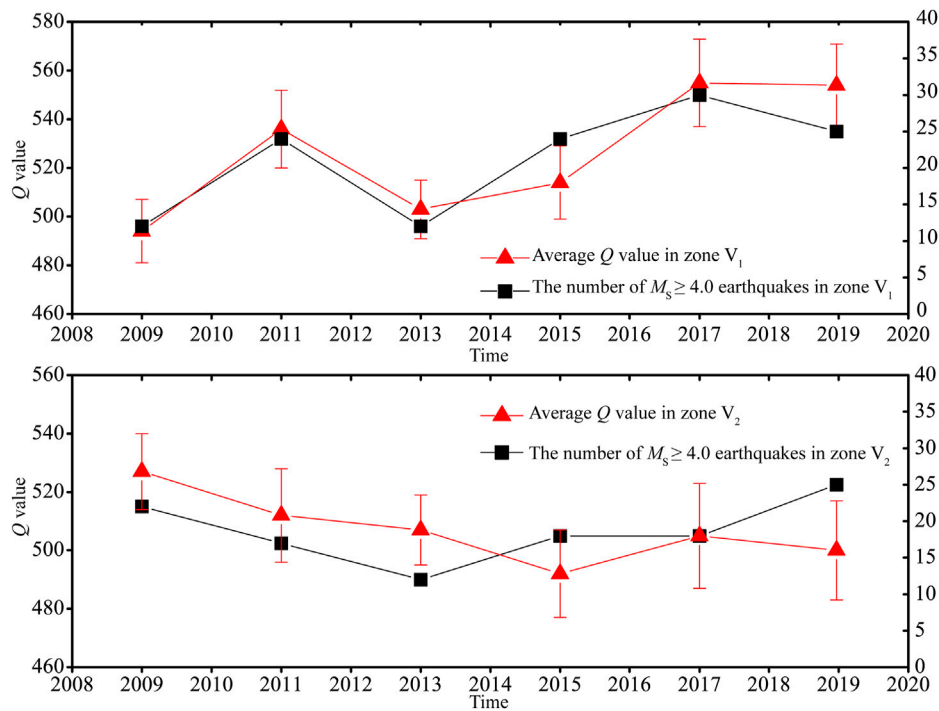
FIGURE 10
Correlation between average Q values and the number of earthquakes in the Tianshan tectonic belt (TTB) over the study period.

propagation of microcracks, until the rock is fractured and changes the regional Q value.

5 Discussion and conclusion

In this study, we performed high-resolution (0.8°×0.8°) Q-tomography for the crust beneath the TTB, *via* attenuation tomography, using 24,273 near-source waveforms collected from 51 digital seismic stations in the Xinjiang regional seismic network from 2009 to 2020. A high-resolution crustal attenuation model of

the TTB was thus, obtained. The major conclusions of this study are explained below.

(1) For the TTB, we observed Q_S values between 300 and 800, with an average Q_0 value of 523. The Q_S value exhibited significant lateral variation, and the distribution of Q_S (and the crustal attenuation structures represented by this distribution) correlated strongly with the TTB's surface tectonics. The main region of the TTB portrayed high Q values (650–750), whereas the areas adjacent to the basins to the south and north and the basin margins exhibited low Q_S values (<550). These

trends reflected the transition from the mountainous regions to the plains and basins, along with the gradual thickening of the sedimentary strata.

The crustal medium in the TTB is associated with high S-wave velocities; however, the Tarim, Junggar, and Turpan Basins are characterized by low wave velocities, as they are covered by thick sedimentary layers (Guo et al., 2010; Tang et al., 2011; Cai et al., 2019; Kong et al., 2021). Low-velocity bodies were observed in many parts of the TTB's middle and upper crust, being predominantly located in the block intersections and mountain-basin transition zones on either side of the Tianshan Mountains (Li et al., 2007). The 3D velocity structure of the crust in the middle Tianshan region revealed a high-velocity zone in the shallow strata and a low-velocity zone in the region close to the Junggar Basin (Zhang et al., 2021). These studies indicated that within the TTB, velocity structures portray a positively correlation with the attenuation structures. The main area of the TTB exhibited high velocities and Q values (low attenuation), whereas the areas adjacent to the basins and the basin margins exhibited low velocities and Q values (high attenuation). This confirmed that 2D attenuation structures were generally consistent with the velocity and 2D density structures (Burtman and Molnar, 1993). Notably, the lateral heterogeneities in the TTB's attenuation structure were mainly caused by the heterogeneities in the crustal medium. In addition, according to the deep structure reported by Xu et al. (2000) for the TTB, an intracrustal low-velocity zone that extends in the NNE direction is present between the southern Tianshan region, Pamir Mountains, and Tarim Basin. This low-velocity zone is flanked by Bachu and Makit (a high-velocity zone) to the east, and Pamir and southern Tianshan to the west. These results generally agree with the distribution of the Q_s values obtained to determine the crustal attenuation structure of southwestern Tianshan for study period (2009–2020) (Figure 7).

(2) Most earthquakes in the TTB of magnitudes ≥6.0 since 1900 (Figure 7) occurred in the transition zones between the high- and low-Q transition zones, or in the low-Q areas. This phenomenon was consistent with the previous observations of the Sichuan–Yunnan region (Pei et al., 2010). Similar phenomena have also been reported in other regions within and outside China (Hansen et al., 2004; Wang et al., 2007; Zhang et al., 2009; Wang et al., 2012a; Qiu et al., 2021). Pei et al. (2010) hypothesize that earthquakes occur most likely in transition zones since the maximum change in the differential stress in rocks occurs in such areas. It has also been proposed that these transition zones tend to accumulate strain (which induces earthquakes) because they are areas where "soft" and "hard" crustal media converge (Wang et al., 2012a).

Previous studies also suggested that strong earthquakes at the junctions between basins and mountains predominantly occur in high-velocity zones in the middle or lower crust, or in the vicinity of areas with large velocity gradients (Zhao et al., 1996; Xu et al., 2000; Zhao et al., 2002; Mukhopadhyay et al., 2006; Wang et al., 2007; Zheng et al., 2007). Based on the results obtained from different regions, heterogeneity in the crustal

medium is a prerequisite for strong earthquakes. Our study results are in agreement with these findings, as most earthquakes of magnitudes ≥6.0 (Figure 7) occurred in transition zones between areas of high and low Q values, or in those having low Q values.

(3) In this study, the average Q_s value of the TTB only varied between 500 and 540 from one period to another, which was consistent with the average Q_0 value (523) for the entire study period (2009–2020). However, the average Q_s values for the middle Tianshan region portrayed a general upward trend since 2009 (from 494 in 2010 to 554 in 2020). By contrast, the average Q_s value for the southwestern Tianshan regions was relatively stable (from 490 to 530) during most periods. The regional average Q value for the middle Tianshan region was higher than that of the southwestern Tianshan region, during most periods (except 2009–2010), which was consistent with the fact that tectonic movements were more intense in the southwestern Tianshan area than the.middle Tianshan region.

(4) The dynamics of the Q value provided insights into the trends pertaining to tectonic activity, rock fracturing, and subsurface fluid flow, serving as a foundation for the understanding of seismogenic mechanisms. By comparing the number of earthquakes and the regional average Q value of the middle and southwestern Tianshan regions, we could deduce that seismic frequency was positively correlated with the regional average Q value. This was consistent with the findings from the Sichuan–Yunnan region (Pei et al., 2010) and Hainan Island and its adjacent areas (Wang et al., 2016), i.e., the greater the regional average Q, the greater the number of earthquakes. The temporal variations in the Q values were related to the tectonic activity trends, and the accumulation and release of stress were essentially the processes through which the earthquakes occurred. Notably, changes in rock stress may cause fractures within the rock to close or open, thus, changing the density of fractures in the rock, ultimately changing the regional Q values (Pei et al., 2010).

Data availability statement

The original contributions presented in the study are included in the article/supplementary material, further inquiries can be directed to the corresponding author.

Author contributions

JL completed the data processing and writing of the manuscript. HJ and QW developed the idea of the manuscript and supported the completion of the manuscript. All authors contributed to the article and approved the submitted version.

Funding

XH22025D and XH21042), and Key Research and Development Program of the Xinjiang Uygur Autonomous Region (Grant Nos. 2022B03001-1 and 2020B03006-3) and Institute of Engineering Mechanics (China Earthquake Administration) Scientic Research (Grant Nos.22020EEEVL0203).

Acknowledgments

Conflict of interest

Publisher's note

References

Abdrakhmatov, K. Y., Aldazhanov, S. A., Hager, B. H., Hamburger, M. W., Herring, T. A., Kalabaev, K. B., et al. (1996). Relatively recent construction of the Tien Shan inferred from GPS measurements of present-day crustal deformation rates. *Nature* 384, 450–453. doi:10.1038/384450a0

Atkinson, G. M., and Mereu, R. F. (1992). The shape of ground motion attenuation curves in southeastern Canada. *Bull. Seismol. Soc. Amer.* 82, 2014–2031. doi:10.1785/bssa0820052014

Avouac, J. P., Tapponnier, P., Bai, M., You, H., and Wang, G. (1993). Active thrusting and folding along the northern tien Shan and late cenozoic rotation of the Tarim relative to dzungaria and Kazakhstan. *J. Geophys. Res.* 98 (B4), 6755–6804. doi:10.1029/92jb01963

Baqer, S., and Mitchell, B. J. (1998). Regional variations of Lg coda Q in the continental United States and its relation to crustal structure and evolution. *Pure Appl. Geophys.* 158, 613–638.

Brune, J. N. (1970). Tectonic stress and the spectra of seismic shear waves from earthquakes. *J. Geophys. Res.* 75 (26), 4997–5009. doi:10.1029/jb075i026p04997

Burtman, V. S., and Molnar, P. (1993). Geological and geophysical evidence for deep subduction of continental crust beneath the Pamir. *Geol. Soc. Am. Inc* 281, 248–251.

Cai, Y., Wu, J. P., Ming, Y. H., Fang, L. H., Wang, W. L., Kong, X. Y., et al. (2019). Crust-mantle S wave velocity structures beneath Tianshan area and its deformation analysis. *Chin. J. Geophys.* 62, 4214–4226. doi:10.6038/cjg2019M0589

Chen, J., Ding, G. Y., Burbank, D. W., Scharer, K., Rubin, C., Sobel, E., et al. (2001). Late cenozoic tectonics and seismicity in the southwestern tianshan China. *Earthq. Res. China* 17, 134–155.

Cong, L. L., Hu, J. F., Fu, Z. W., Wen, Y. B., Kang, G. F., Wu, X. P., et al. (2002). Distribution of Lg cada Q in the Chinese continent and its adiacent regions. *Sci. China Earth Sci.* 32, 617–624.

Cormier, V. F. (1982). The effect of attenuation on seismic body waves. *Bull. Seis Soc. Amer* 72, 169–200.

Deev, E. V., and Korzhenkov, A. M. (2016). Paleoseismological studies in the epicentral area of the 1911 Kemin earthquake (northern Tien Shan). *Russ. Geol. Geophys.* 57, 337–343. doi:10.1016/j.rgg.2016.02.010

Deng, Q. D., Feng, X. Y., and You, H. C. (1991). "Characteristics and mechanism of deformation along the Dushanzi-Anjihai active reverse fault and fold zone, Xinjiang," in *Research on active fault* (Beijing: Seismic Publishing House), 17–36.

Feng, X. Y. (1985). Seismogeological characteristics of the Xinjiang area. *Seismol. Geol.* 7, 35–44.

Gao, G. Y., Nie, X. H., and Long, H. Y. (2010). Discussion on the characteristics of regional tectonic stress field of Xinjiang Fron 2003-2008. *Seismol. Geol.* 32, 70–79. doi:10.3969/j.issn.0253-4967.2010.01.007

Gao, R., Xiao, X. C., Gao, H., Li, Q. S., Liu, X., Jiang, M., et al. (2002). Summary of deep seismic probing of the lithospheric structure across the west Kunlun-Tarim-Tianshan. *Geol. Bull. China* 21, 11–18.

Guo, B., Liu, Q. Y., Chen, J. H., Zhao, D. P., Li, S. C., and Lai, Y. G. (2006). Seismic tomography of the crust and upper mantle structure underneath the Chinese Tianshan. *Chin. J. Geophys.* 49, 1543–1551. doi:10.1002/cjg2.982

Guo, Z., Gao, X., Wang, W. M., Li, G. L., Duan, Z. Q., and Shi, H. (2010). S-wave velocity of the crust around Tianshan Mountains inverted from seismic ambient noise tomography. *Chin. Sci. Bull.* 55, 3590–3598. doi:10.1007/s11434-010-4017-3

Haberland, C., and Rietbrock, A. (2001). Attenuation tomography in the Western central andes: A detailed insight into the structure of a magmatic arc. *J. Geophys. Res.* 106 (B6), 11151–11167. doi:10.1029/2000jb900472

Hansen, S., Thurber, C., Mandernach, M., Haslinger, F., and Doran, C. (2004). Seismic velocity and attenuation structure of the east rift zone and south Flank of Kilauea volcano, Hawaii. *Bull. Seis Soc. Amer* 94, 1430–1440. doi:10.1785/012003154

Hao, Z. B., Qin, J. X., and Wu, X. Y. (2009). Overview of research on the seismic wave quality factor (Q). *Prog. Geophys.* 24, 375–381. doi:10.3969/j.issn.1004-2903.2009.02.002

Haydar, J., Ai-Shukriand Mitchell, B. J. (1990). Three dimensional attenuation structure in and around the new Madrid seismic zone. *Bull. Seis Soc. Amer* 80, 615–632.

He, J., Sandvol, E., Wu, Q. J., Gao, M. T., Gallegos, A., Ulziibat, M., et al. (2017). Attenuation of regional seismic phase (Lg and Sn) in eastern Mongolia. *Geophys. J. Int.* 211 (2), 1001–1011. doi:10.1093/gji/ggx349

Hearn, T. M., Beghoul, N., and Barazangi, M. (1991). Tomography of the Western United States from regional arrival times. *J. Geophys. Res.* 96, 16369–16381. doi:10.1029/91jb01509

Hearn, T. M., Wang, S. Y., Pei, S. P., Xu, Z. H., Ni, J. F., and Yu, Y. X. (2008). Seismic amplitude tomography for crustal attenuation beneath China. *Geophys. J. Int.* 174, 223–234. doi:10.1111/j.1365-246x.2008.03776.x

Hu, J. (2020). Development of regional-scaleseismic velocity and attenuation tomography methods and its applications. [Ph. D. thesis]. Hefei: University of Science and Technology of China.

Hu, J. F., Cong, L. L., Su, Y. J., and Kang, G. F. (2003). Distribution characteristics of q value of the Lg coda in Yunnan and its adjacent regions. *Chin. J. Geophys.* 46, 809–813.

Jiang, H., Gao, M. T., Yu, Y. X., and Tang, L. H. (2007). S wave inelastic attenuation and site effect in the northern Tianshan area. *Acta Seismol. Sin.* 29, 181–186.

Johnston, D. H., Toksoz, M. N., and Timur, A. (2012). Attenuation of seismic waves in dry and saturated rocks: II. Mechanisms. *Geophysics* 44, 691–711. doi:10.1190/1.1440970

Jolivet, M., Dominguez, S., Charreau, J., Chen, Y., Li, Y. G., and Wang, Q. C. (2010). Mesozoic and Cenozoic tectonic history of the central Chinese Tian Shan: Reactivated tectonic structures and active deformation. *Tectonics* 29, TC6019. doi:10.1029/2010tc002712

Kong, X. Y., Wu, J. P., and Liu, J. (2021). S-wave velocity structure inversed by ambient noise tomography in Xinjiang Tienshan and its surrounding areas. *Earthq. Res. China* 37, 43–58.

Kumar, P., Yuan, X., Kind, R., and Kosarev, G. (2005). The lithosphere-asthenosphere boundary in the tien Shan-karakoram region from S receiver functions: Evidence for continental subduction. *Geophys. Res. Lett.* 32, L07305. doi:10.1029/2004GL022291

Larson, K. M., Burgmann, R., Bilham, R., and Freymueller, J. T. (1999). Kinematics of the India-Eurasia collision zone from GPS measurements. *J. Geophys. Res.* 104, 1077–1093. doi:10.1029/1998jb900043

Larson, K. M., Palu, B., and Joan, G. (2003). Using 1-Hz GPS data to measure deformations caused by the Denali fault earthquake. *Science* 300, 1421–1424. doi:10.1126/science.1084531

Li, A., Ran, Y. K., Liu, G. H., and Xu, X. L. (2016). Active characteristics and paleo earthquakes in the west Kalpin nappe since the Holocene, SW Tianshan Mountain. *Adv. Earth Sci.* 31, 377–390. doi:10.11867/j.issn.1001-8166.2016.04.0377

Li, J., Zhou, L. Q., Wang, H. L., and Xiang, Y. (2017). Tomograpgy for Q of eastern section of the Tianshan area from high-frequency attenuation of S wave. *Earthq. Res. China* 33, 229–238.

Li, Y., Liu, Q. Y., Chen, J. H., Li, S. C., Guo, B., and Lai, Y. G. (2007). Shear wave velocity structure of the crust and upper mantle underneath the Tianshan orogenic belt. *Sci. China Earth Sci.* 50, 321–330. doi:10.1007/s11430-007-0008-x

Li, Z. H., Zhu, C. Y., Xia, A. G., Feng, L., and Tang, L. L. (2010). Study on non-elasticity attenuation, site response and source parameters in the Jiashi region. *Xinjiang. Earthq. Res. China* 26, 340–348.

Liu, J. H., Liu, F. T., Yan, X. W., Xu, Y., and Hao, T. Z. (2004b). A study of Lg coda attenuation beneath north China: Seismic imaging of Lg coda Q_0. *Chin. J. Geophys.* 247, 1044–1052.

Liu, J. H., Xu, Y., and Hao, T. Y. (2004a). Study on physical mechanism of the seismic wave attenuation. *Prog. Geophys.* 19, 1–7.

Liu, J., Liu, Q. Y., Guo, B., and Song, H. Z. (2007). Small-scale upper mantle convection and orogeny of Tianshan Mountains in China. *Sci. China Earth Sci.* 50, 1142–1149. doi:10.1007/s11430-007-0070-4

Liu, J. M., and Li, Z. H. (2014). Non-elastic attenuation, site response and source parameters in the Northern Tianshan Mountain, Xinjiang of China. *Earthquake* 34, 77–86.

Liu, J., Zheng, S. H., and Huang, Y. L. (2003). The inversion of non-elasticity coefficient, source parameters, site response using genetic algorithms. *Acta Seismol. Sin.* 25, 211–218.

Liu, Y. H., Liu, X. W., Yang, X., Zheng, J. J., Wang, Y. D., and Su, L. (2012). Discussion of some problems of plate tectonics evolution and mantle dynamics of Tianshan and its adjacent area. *J. Geod. Geodynam.* 32, 31–37.

Liu, Y. H., Liu, X. W., Zheng, J. J., Zhao, D. D., Yang, X., and Wang, Y. D. (2011). Coupling dynamic mechanisms between plate tectonics evolution and mantle convection of south and north Tianshan. *Prog. Geophys.* 26, 1544–1556. doi:10.3969/j.issn.1004-2903.2011.05.006

Lu, D. Y., Li, Q. S., Gao, R., Li, Y. K., Li, D. X., Liu, W., et al. (2000). A deep seismic sounding profile across the Tianshan Mountains. *Chin. Sci. Bull.* 45, 2100–2107. doi:10.1007/bf03183536

Ma, H. S., Wang, S. Y., Pei, S. P., Liu, J., Hua, W., and Zhou, L. Q. (2007). Q_0 tomography of S wave attenuation in Sichuan, Yunnan and adjacent regions. *Chin. J. Geophys.* 50, 423–429. doi:10.1002/cjg2.1051

Mitchell, B. J. (1995). Anelastic structure and evolution of the continental crust and upper mantle from seismic surface wave attenuation. *Rev. Geophys.* 33, 441–462. doi:10.1029/95rg02074

Mitchell, B. J., Pan, Y., Xie, J. K., and Cong, L. L. (1997). Lg coda Q variation across Eurasia and its relation to crustal evolution. *J. Geophys. Res.* 102, 22767–22779. doi:10.1029/97jb01894

Molnar, P., and Lyon-Caen, H. (1989). Fault plane solution of earthquakes and active tectonics of the Tibetan Plateau and its margins. *Geophys. J. Int.* 99, 123–153.

Molnar, P., and Tapponnier, P. (1978). Active tectonics of tibet. *J. Geophys. Res.* 83, 5361–5374. doi:10.1029/jb083ib11p05361

Molnar, P., and Tapponnier, P. (1975). Cenozoic Tectonics of Asia: Effects of a Continental Collision: Features of recent continental tectonics in Asia can be interpreted as results of the India-Eurasia collision. *Science* 189, 419–426. doi:10.1126/science.189.4201.419

Mukhopadhyay, S., Mishra, O. P., Zhao, D., and Kayal, J. R. (2006). 3-D seismic structure of the source area of the 1993 Latur, India, earthquake and its implications for rupture nucleations. *Tectonophysics* 415, 1–16. doi:10.1016/j.tecto.2005.10.041

Pei, S. P., Liu, J., Ma, H. S., Gao, X., and Su, J. R. (2010). Dynamic variation of S-wave Q value beneath Sichuan-Yunnan, China. *Chin. J. Geophys.* 53, 1639–1652. doi:10.3969/j.issn.0001-5733.2010.07.015

Pei, S. P., Su, J. R., Gao, X., Zhao, J. M., and Liu, H. B. (2008). S-wave attenuation tomography of upper crust in Japan. *Chin. J. Geophys.* 51, 828–835.

Pei, S. P., Zhao, J. M., Rowe, C. A., Wang, S. Y., Hearn, T. M., Xu, Z. H., et al. (2006). M-L amplitude tomography in north China. *Bull. Seis Soc. Amer.* 96, 1560–1566. doi:10.1785/0120060021

Qiu, Y. R., Yang, Y. H., Shao, H. C., and Zhang, E. H. (2021). Crustal Q_S tomography in intersection area of shaanxi-gansu-ningxia. *Earthq. Res. China* 37, 95–106.

Qu, Y. J., Wang, Q., and Nie, X. H. (2010). Research on the structural belts and earthquake activity state in the south part of Xinjiang. *Inland Earthq.* 24, 298–306.

Ran, Y. K., Yang, X. P., Xu, X. W., Chen, J. W., and Chen, L. C. (2006). Deformation pattern and shortening rates in the east part of kalpin thrust system in southwest Tianshan during late quaternary. *Seismol. Geol.* 28, 179–193.

Reigber, C., Michel, G. W., Galas, R., Angermann, D., Klotz, J., Chen, J. Y., et al. (2001). New space geodetic constraints on the distribution of deformation in Central Asia. *Earth Planet. Sci. Lett.* 191, 157–165. doi:10.1016/s0012-821x(01)00414-9

Roecker, S. W., Sabitova, T. M., Vinnik, L. P., Burmakov, Y. A., Golvanov, M. I., Mamatkanova, R., et al. (1993). Three-dimensional elastic wave velocity structure of the Western and central Tien Shan. *J. Geophys. Res.* 98, 15779–15795. doi:10.1029/93jb01560

Romanowicz, B. (1994). On the measurement of anelastic attenuation using amplitudes of low frequency surface waves. *Phys. Earth Planet. Inter.* 84, 179–191. doi:10.1016/0031-9201(94)90040-x

Romanowicz, B. (1990). The upper mantle degree 2: Constraints and inferences from global mantle wave attenuation measurements. *J. Geophys. Res.* 95, 11051–11071. doi:10.1029/jb095ib07p11051

Sanders, C. O. (1993). "Local earthquake tomography: Attenuation theory and results," in *Seismic Tomography: theory and Practice* (New York: Chapman & Hall), 676–694.

Scholz, C. H. (2002). *The mechanics of earthquakes and faulting.* 2nd ed. Cambridge: Cambridge Univ. Press.

Schubert, G., Turcott, D. L., and Olsen, P. (2001). *Mantle convection in the earth and planets.* Oxford: Cambridge University Press.

Shao, X. Z., Zhang, J. R., Fan, H. J., Zheng, J. D., Xu, Y., Zhang, H. Q., et al. (1996). The crust structures of tianshan orogenic belt: A deep sounding work by converted waves of earthquakes along rmqi-korla profile. *Chin. J. Geophys.* 39, 336–346.

Sherbaum, F. (1990). Combined inversion for the three-dimensional Q structure and source parameters using microearthquake spectra. *J. Geophys. Res.* 95, 12423–12438. doi:10.1029/jb095ib08p12423

Shu, L. S., Guo, Z. J., Zhu, W. B., Lu, H. F., and Wang, B. (2004). Post-collision tectonism and basin-range evolution in the tianshan belt. *Geol. J. China Univ.* 10, 393–404.

Su, Y. J. (2009). Inversion tomography of the seismic wave attenuation (Q value) structure in Yunnan region. [Ph. D. thesis]. Hefei: University of Science and Technology of China.

Su, Y. J., Liu, J., Zheng, S. H., Liu, L. F., Fu, H., and Xu, Y. (2006). Q value of anelastic S-wave attenuation in Yunnan region. *Acta Seismol. Sin.* 28, 206–212.

Sun, L., Li, Y. H., Wu, Q. J., and Wang, S. Y. (2012). Q_0 tomography of S wave attenuation in Northeast China and adjacent regions. *Chin. J. Geophys.* 55, 1179–1185. doi:10.6038/j.issn.0001-5733.2012.04.014

Tang, L. L., Kong, X. Y., Long, F., and Feng, J. G. (2013). Identification and spatio-temporal characteristics of re-peating earthquakes in Kepingtage fault zone. *Acta Seismol. Sin.* 35, 328–340. doi:10.3969/j.issn.0253-3782.2013.03.005

Tang, X. Y., Fan, W. Y., Feng, Y. G., Tang, Y. C., Chen, Y. S., and Zhu, L. X. (2011). Phase velocity tomography of Rayleigh wave in Xinjiang from ambient noise. *Chin. J. Geophys.* 54, 2042–2049. doi:10.3969/j.issn.0001-5733.2011.08.011

Tapponnier, P., and Molnar, P. (1979). Active faulting and cenozoic tectonics of the tien Shan, Mongolia, and baykal regions. *J. Geophys. Res.* 84, 3425–3459. doi:10.1029/jb084ib07p03425

Tapponnier, P., and Molnar, P. (1977). Active faulting and tectonics in China. *J. Geophys. Res.* 82, 2905–2930. doi:10.1029/jb082i020p02905

Toksoz, M. N., Johnston, D. H., and Timur, A. (1979). Attenuation of seismic waves in dry and saturated rocks: I. Laboratory measurements. *Geophysics* 44, 681–690. doi:10.1190/1.1440969

Walsh, J. B. (1966). Seismic wave attenuation in rock due to friction. *J. Geophys. Res.* 71, 2591–2599. doi:10.1029/jz071i010p02591

Wan, Y. G., Shen, Z. K., Sheng, S. Z., and Xu, X. F. (2009). The influence of 2008 Wenchuan earthquake on surrounding faults. *Acta Seismol. Sin.* 31, 128–139.

Wang, H. L., Xu, X. F., Zhou, L. Q., Zhang, X. D., Shen, F. L., Li, Z. X., et al. (2016). Crustal Qs tomography in hainan Island and adjacent region. *Seismol. Geol.* 38, 631–645. doi:10.3969/j.issn.0253-4967.2016.03.010

Wang, H. L., Zhang, X. D., Zhou, L. Q., and Xu, X. F. (2012b). Relationship between the reservoir storage and crustal Q_S dynamic variation in Zipingpu reservoir area. *Acta Seismol. Sin.* 34, 676–688. doi:10.3969/j.issn.0253-3782.2012.05.009

Wang, H. L., Zhang, X. D., Zhou, L. Q., Xu, X. F., Yang, Z. G., Lu, X., et al. (2012a). Study on the relationship between fluid infiltration and Q_S tomography of the crust in Zipingpu Reservoir Area. *Chin. J. Geophys.* 55, 526–537. doi:10.6038/j.issn.0001-5733.2012.02.015

Wang, Q., Ding, G. Y., Qiao, X. J., Wang, X. Q., and You, X. Z. (2000). Recent rapid shortening of crust across the Tianshan Mts. and relative motion of tectonic blocks in the north and south. *Chin. Sci. Bull.* 45, 1995–1999. doi:10.1007/bf02909695

Wang, Q., Qu, Y. J., and Nie, X. H. (2011). Analysis on seismicity state of tectonic regions in the northern part of Xinjiang. *Northwest. Seismol. J.* 33, 137–142.

Wang, S. Y., Pei, S. P., Thomas, M. H., Xu, Z. H., James, F. N., and Yu, Y. X. (2008). Crustal S-wave Q estimated from ML amplitude II: Q lateral variation in China. *Chin. J. Geophys.* 51, 133–139.

Wang, S. Y., Pei, S. P., Xu, Z. H., Zhang, G. M., Yu, Y. X., and Pan, H. (2007a). Crustal S wave Q estimated from ML amplitude I: Attenuation in different tectonic regions of China. *Chin. J. Geophys.* 50, 1740–1747. doi:10.3321/j.issn:0001-5733.2007.06.014

Wang, W. J., Chen, L., Chen, Q. F., and Liu, J. (2007b). Velocity and attenuation structures in the focal area of 2003 Dayao earthquakes. *Chin. J. Geophys.* 50, 686–696. doi:10.1002/cjg2.1082

Wessel, P., and Smith, W. H. F. (1995). New version of the generic mapping tools. *EOS Trans. AGU* 76, 329. doi:10.1029/95eo00198

Winkler, K., and Nur, A. (1979). Pore fluids and seismic attenuation in rocks. *Geophys. Res. Lett.* 6, 1–4. doi:10.1029/gl006i001p00001

Wittlinger, G. H., Haessler, H., and Granet, M. (1983). Three dimensional inversion of Q_P from low magnitude earthquakes analysis. *Ann. Geophys.* 6, 427–438.

Xiao, X. C., Liu, X., and Gao, R. (2004). *The crustal structure and tectonic evolution of southern Xinjiang*. China. Beijing: The Commercial Press.

Xiong, X. S., Gao, R., Li, Q. S., Wang, H. Y., Lu, Z. W., and Hou, H. S. (2011). The deep structure of Tienshan orogenic belt. *Prog. Geophys.* 26, 1906–1914. doi:10.3969/j.issn.1004-2903.2011.06.003

Xu, Y., Liu, F. T., Liu, J. H., and Sun, R. M. (2000). Crustal structure and tectonic environment of strong earthquakes in the Tianshan earthquake belt. *Chin. J. Geophys.* 43, 184–193.

Yang, S. M., Li, J., and Wang, Q. (2008). The deformation pattern and fault rate in the Tianshan Mountains inferred from GPS observations. *Sci. China Earth Sci.* 51, 1064–1080. doi:10.1007/s11430-008-0090-8

Yang, X. P., Ran, Y. K., Song, F. M., Xu, X. W., Chen, J. W., Min, W., et al. (2006). The analysis for crust shortening of kalpin thrust tectonic zone, south-Western tianshan, Xinjiang, China. *Seismol. Geol.* 28, 194–204.

Ye, Q. D., Yan, C. H., Wang, S. W., Mao, Y. F., Yu, D. X., and Yan, L. L. (2018). Crustal 2-D Q_S tomography in Longtan reservoir,Guangxi region. *Acta Seismol. Sin.* 40, 689–700. doi:10.11939/jass.20170227

Yi, G. X., Wen, X. Z., Xin, H., Qiao, H. Z., and Gong, Y. (2013). Stress state and major-earthquake risk on the southern segment of the Longmen Shan fault zone. *Chin. J. Geophys.* 56, 1112–1120. doi:10.6038/cjg20130407

Yin, A., Nie, S., Craig, P., Harrison, T. M., Ryerson, F. J., Qian, X. L., et al. (1998). Late Cenozoic tectonic evolution of the southern Chinese Tian Shan. *Tectonics* 17, 1–27. doi:10.1029/97tc03140

Zhang, J. Q., Liu, J., and Zhou, L. Q. (2009). Tomography and analysis of velocity and attenuation structure for the 2000 Yaoan aftershock tomography and analysis of velocity and attenuation structure for the 2000 Yaoan aftershock area in Yunnan. *Earthquake* 29, 126–135.

Zhang, P. Z., Deng, Q. D., Yang, X. P., Peng, S. Z., Xu, X. W., and Feng, X. Y. (1996). Late cenozoic tectonic deformation and mechanism along the tianshan Mountain,Northwestern China. *Earthq. Res. China* 12, 127–140. doi:10.3969/j.issn.0001-5733.2011.06.007

Zhang, P. Z., Deng, Q. D., Zhang, G. M., Ma, J., Gan, W. J., Min, W., et al. (2003). Strong earthquake activity and active blocks in Chinese Mainland. *Sci. China Earth Sci.* 33, 12–20. doi:10.3321/j.issn:1006-9267.2003.z1.002

Zhang, Z. B., Liang, X. F., Zhou, B. B., Liu, D. Q., and Tang, M. S. (2021). Three-dimensional seismic velocity structure of the middle part of north Tianshan mountains, Xinjiang based on seismic relocation and local seismic tomography. *Seismol. Geol.* 43, 1292–1310. doi:10.3969/j.issn.0253-4967.2021.05.015

Zhao, C. P., Chen, Z. L., Zheng, S. H., and Zhang, Z. Q. (2008). Moment inversion of moderate earthquakes and the locally perturbed stress field in the Jiashi source region. *Chin. J. Geophys.* 51, 782–792. doi:10.3321/j.issn:0001-5733.2008.03.019

Zhao, C. P., Chen, Z. L., Hua, W., Wang, Q. C., Li, Z. X., and Zheng, S. H. (2011). Study on source parameters of small to moderate earthquakes in the main seismic active regions, China mainland. *Chin. J. Geophys.* 54, 1478–1489. doi:10.3969/j.issn.0001-5733.2011.06.007

Zhao, D. P., Kanamori, H., Negishi, H., and Wiens, D. (1996). Tomography of the source area of the 1995 Kobe earthquake: Evidence for fluids at the hypocenter? *Science* 274, 1891–1894. doi:10.1126/science.274.5294.1891

Zhao, D. P., Mishra, O. P., and Sanda, R. (2002). Influence of fluids and magma on earthquakes: Seismological evidence. *J. Geophys. Res.* 132, 249–267. doi:10.1016/s0031-9201(02)00082-1

Zhao, J. M., Zhang, P. Z., Zhang, X. K., Yuan, X. H., Rainer, K., Robert, V. D., et al. (2021). Crust-mantle structure and geodynamic processes in Western China and their constraints on resources and environment: Research progress of the ANTILOPE Project. *Earth Sci. Front.* 28, 230–259. doi:10.13745/j.esf.sf.2021.9.38

Zheng, J. C., Gu, J. P., and Zhang, Y. S. (2007). Combined Inversion of the upper crust 3-D velocity structure in north China. *Prog. Geophys* 22 (06), 1706–1714.

Zhou, L. Q., Liu, J., Su, Y. J., Ma, H. S., and Zhou, J. J. (2009). Tomography for Q of Yunnan region from high-frequency attenuation of S wave. *Chin. J. Geophys.* 52, 1500–1507. doi:10.3969/j.issn.0001-5733.2009.06.011